

**The large-scale anomalous microwave emission revisited
by WMAP**
Guilaine Lagache

► **To cite this version:**

Guilaine Lagache. The large-scale anomalous microwave emission revisited by WMAP. *Astronomy and Astrophysics - A&A*, EDP Sciences, 2003, 405 (3), pp.813 - 819. 10.1051/0004-6361:20030545 . hal-01840640

HAL Id: hal-01840640

<https://hal-amu.archives-ouvertes.fr/hal-01840640>

Submitted on 16 Jul 2018

HAL is a multi-disciplinary open access archive for the deposit and dissemination of scientific research documents, whether they are published or not. The documents may come from teaching and research institutions in France or abroad, or from public or private research centers.

L'archive ouverte pluridisciplinaire **HAL**, est destinée au dépôt et à la diffusion de documents scientifiques de niveau recherche, publiés ou non, émanant des établissements d'enseignement et de recherche français ou étrangers, des laboratoires publics ou privés.

The large-scale anomalous microwave emission revisited by WMAP[★]

G. Lagache^{★★}

IAS, Bât. 121, Université Paris-Sud, 91435 Orsay, France

Received 24 March 2003 / Accepted 8 April 2003

Abstract. We present a new study of the high latitude galactic contributions to the millimeter sky, based on an analysis of the *WMAP* data combined with several templates of dust emission (*DIRBE/COBE* and *FIRAS/COBE*) and gas tracers (HI and H_α). To study the IR to millimeter properties of the diffuse sky at high galactic latitude, we concentrate on the emission correlated with the HI gas. We compute the emission spectrum of the dust/free-free/synchrotron components associated with HI gas from low to large column densities. A significant residual *WMAP* emission over the free-free, synchrotron and the dust contributions is found from 3.2 to 9.1 mm. We show that this residual *WMAP* emission (normalised to 10^{20} atoms/cm²) (1) exhibits a constant spectrum from 3.2 to 9.1 mm and (2) significantly decreases in amplitude when N_{HI} increases, contrary to the HI -normalised far-infrared emission which stays rather constant. It is thus very likely that the residual *WMAP* emission is not associated with the Large Grain dust component. The decrease in amplitude with increasing opacity resembles in fact to the decrease of the transiently heated dust grain emission observed in dense interstellar clouds. This is supported by an observed decrease of the HI -normalised $60\ \mu\text{m}$ emission with HI column densities. Although this result should be interpreted with care due to residual zodiacal contaminations at $60\ \mu\text{m}$, it suggests that the *WMAP* excess emission is associated with the small transiently heated dust particles. On the possible models of this so-called “anomalous microwave emission” linked to the small dust particles are the spinning dust and the excess millimeter emission of the small grains, due to the cold temperatures they can reach between two successive impacts with photons.

Key words. ISM: general – cosmology: miscellaneous – radio continuum: general

1. Introduction

At millimeter wavelengths, one of the major challenges in high sensitivity Cosmic Microwave Background (CMB) anisotropy study is to determine the fraction of the observed signal due to diffuse galactic foregrounds. Three different components have been firmly identified at high latitudes ($|b| > 10^\circ$): thermal dust emission, synchrotron and free-free. Dust emission dominates the far-infrared surveys. Its spatial distribution and frequency dependence are quite well-determined for wavelengths shorter than $\sim 800\ \mu\text{m}$. Above $\sim 800\ \mu\text{m}$, present data currently do not give any strong constraints. So far, dust emission estimates in the millimeter range are thus an extrapolation of what is known at shorter wavelengths. Synchrotron radiation dominates radio-frequency surveys, but Banday & Wolfendale (1991) and Bennett et al. (1992) showed that the spectral index steepens with frequency and exhibits spatial variations which are poorly known. Free-free emission has a well-determined spectral behavior and templates are now available thanks to the *WHAM* H_α survey of the northern sky (Reynolds et al. 1998;

Haffner 1999) and the *SHASSA* H_α survey of the southern sky (Gaustad et al. 2001).

Cross-correlations of CMB data with far-infrared maps have revealed the existence of a microwave emission component (the so-called “anomalous microwave emission”) with spatial distribution traced by these maps. This component has a spectral index suggestive of free-free emission and so has been first interpreted as free-free emission (Kogut et al. 1996). However, Kogut (1999) showed in small parts of the sky that were covered by H_α data that the microwave emission was consistently brighter than the free-free emission traced by H_α . Thus, the correlated component cannot be due to free-free emission alone. This is confirmed more recently by Banday et al. (2003) also using *COBE/DMR* data.

Recent works suggest that this anomalous far-infrared correlated component originates from spinning dust grain emission (Draine & Lazarian 1998a; De Oliveira-Costa et al. 1999, 2002), tentatively detected at 5, 8 and 10 GHz by Finkbeiner et al. (2002). An alternative explanation is provided by thermal fluctuations in the magnetization of interstellar grains causing magnetic dipole radiation (Draine & Lazarian 1999). However, very recently, Bennett et al. (2003) using *WMAP* data do not find any evidence for the anomalous microwave emission. Their foreground component model comprises only free-free, synchrotron and thermal dust emission, and the observed

[★] The Wilkinson Microwave Anisotropy Probe (*WMAP*) is the result of a partnership between Princeton University and NASA's Goddard Space Flight Center.

^{★★} e-mail: Guilaine.Lagache@ias.u-psud.fr

galactic emission matches the model to <1%. Note that in their global analysis, they are dominated by the brightest parts of the sky i.e. the galactic plane and the high latitude dense interstellar clouds. Thus, results may not apply to the most diffuse regions.

We present in this paper a new study of the galactic contributions to the millimeter sky, based on an analysis of the *WMAP* data combined with several templates of dust emission (*DIRBE/COBE* and *FIRAS/COBE*) and gas tracers (HI and H_α). We focus only on the high latitude regions where the results are easier to interpret in term of physical properties of dust and where CMB analysis are performed. The paper is organised as follows. We first present the data we use together with their preparation (Sect. 2). We then derive the spectrum (from 100 μm to 10 mm) of the HI-correlated component (Sect. 3.1) and show that there exists a residual microwave emission (over free-free, synchrotron and far-infrared dust emission) whose HI-normalised amplitude decreases when the HI column density increases but without any significant spectral variations (Sect. 3.2). We then discuss the results in Sect. 4.

2. Data-sets used and their preparation

2.1. COBE data

The *COBE* satellite was developed by NASA’s Goddard Space Flight Center to measure the diffuse infrared and microwave radiation from the early universe to the limits set by our astrophysical environment. It was launched November 18, 1989 and carried three instruments:

- a Far Infrared Absolute Spectrophotometer (*FIRAS*) to compare the spectrum of the cosmic microwave background radiation with a precise blackbody (at each sky position, with an angular resolution of 7° , we have one spectrum from 1 to 97 cm^{-1});
- a Differential Microwave Radiometer (*DMR*) to map the cosmic radiation (at 31, 53, 90 GHz with a 7° beam);
- a Diffuse Infrared Background Experiment (*DIRBE*) to search for the cosmic infrared background radiation (10 photometric bands from 1 to 240 μm with an angular resolution of $40'$).

COBE data are presented in a quadrilateralized spherical projection (the so-called *COBE* Quadrilateralized Spherical Cube, CSC), an approximately equal-area projection in which the celestial sphere is projected onto an inscribed cube. The *DIRBE* convention is to divide each cube face into 256×256 pixels; thus all sky-maps have $256 \times 256 \times 6 = 393\,216$ pixels. Each pixel is approximately 0.32° on a side. For *FIRAS* and *DMR*, each cube face is 32×32 pixels leading to a total of 6144 pixels (of $\sim 2.6^\circ$).

We use the so-called (i) “Sky Maps and Analyzed Science Data Sets” *DMR* Data (ii) “Galactic Dust Continuum Spectra and Interstellar Dust Parameters” *FIRAS* data, that give the residual sky spectrum after modelled emission from the CMB, zodiacal emission, and interstellar lines have been subtracted. (iii) *DIRBE* “Zodi-Subtracted Mission

Average (ZSMA) Maps” for which the zodiacal light intensities were subtracted week by week and the residual intensity values were averaged to create Maps. All *COBE* data are available at <http://lambda.gsfc.nasa.gov/product/cobe>

2.2. Gas tracers

The HI data we used are those of the Leiden/Dwingeloo survey which covers the entire sky down to $\delta = -30^\circ$ with a grid spacing of $30'$ in both l and b. The $36'$ half power beam width of the Dwingeloo 25 m telescope provides 21 cm maps at an angular resolution which closely matches that of the *DIRBE* maps. Details of the observations and correction procedures are given by Hartmann (1994) and by Hartmann & Burton (1997). It should be noted that in this data-set special care was taken for the removal of far sidelobes emission which makes it particularly suitable for high latitude studies. We derive the HI column densities using $1 \text{ K km s}^{-1} = 1.82 \times 10^{18} \text{ H cm}^{-2}$ (optically thin emission).

Thanks to the *WHAM* survey of the northern sky (Reynolds et al. 1998; Haffner 1999) and the *SHASSA* survey of the southern sky (Gaustad et al. 2001), it is now possible to have a whole sky map of the H_α emission (Dickinson et al. 2003; Finkbeiner 2003). Since the HI maps cover the sky down to $\delta = -30^\circ$, the H_α emission we use in our analysis is mostly given by the *WHAM* survey. *WHAM* provides a 12 km s^{-1} velocity resolution with one-degree angular resolution down to sensitivity limits of $0.2 R$ ($1 R = 10^6/4\pi \text{ ph cm}^{-2} \text{ s}^{-1} \text{ sr}^{-1}$) in a 30 second exposure. The one-degree angular resolution nicely matches the *DIRBE* resolution. We use the H_α map and the conversion factors to free-free emission (using $T_e = 8000 \text{ K}$) from Finkbeiner (2003) to derive templates of free-free emission. Since we work only on high latitude regions, the H_α emission has not been corrected for extinction (the dust absorption is likely to be very small, less than 5%). The free-free templates are used to derive a well-understood contribution to the millimeter channels.

2.3. Synchrotron templates

Synchrotron emission arises from relativistic cosmic ray electrons spiralling in the galactic magnetic field. This emission dominates surveys at radio frequencies. The only all-sky map at low frequencies that probe the synchrotron emission is the 408 MHz survey of Haslam et al. (1982). For many years, this map has been used to predict the synchrotron emission in the millimeter channels, assuming a frequency dependence with a constant spectral index of about 2.75. However, Bennett et al. (2003) have shown that the synchrotron spectral index exhibit strong spatial variations and is steeper in the *WMAP* bands than at radio frequencies. We thus use the *WMAP* synchrotron maps derived by Bennett et al. (2003) using the Maximum Entropy Method as frequency dependent well-determined synchrotron templates.

2.4. *WMAP* data

The *WMAP*¹ (Wilkinson Microwave Anisotropy Probe) mission, designed to determine the geometry, content, and evolution of the universe, has successfully provided full sky maps at 23, 33, 41, 61 and 94 GHz at respectively 13.2, 39.6, 30.6, 21 and 13.2' FWHM resolution with unprecedented sensitivity. A detailed description of the delivered data-sets for the first 12 months of operation of *WMAP* is given in the *WMAP: explanatory Supplement* (editor M. Limon et al., Greenbelt, MD: NASA/GSFC). The data we use are the first-year “Smoothed I maps” which are the temperature maps at each frequency, smoothed to a common resolution of 1 degree. Data are delivered in the HEALPix² format with $N_{\text{side}} = 256$.

2.5. Data preparation

All the data have to be put in the same projection and at the same resolution. The resolution is set by the *FIRAS* experiment since it is the lowest resolution of our data-sets (7°). All data but *DMR* and *FIRAS* are thus converted in the *DIRBE* CSC format and then convolved with the *FIRAS* beam and degraded to the *FIRAS* CSC resolution (see Lagache 2003 for more details).

We have removed for each data-set the cosecant law variation (1) to avoid the obvious large scale correlations between all galactic components concentrated in the disc and (2) to be consistent with the *WMAP* data that measure only differentially on the sky and thus does not measure the largest angular scales.

We restrict our analysis to $|b| > 15^\circ$ and exclude the Small and Large Magellanic clouds, together with the ρ -Ophiucus complex. We also remove cold molecular complexes (as the Taurus cloud), and regions where the dust is locally heated by nearby stars (like the HII regions) following Lagache et al. (1998). We stress out that this latter pixel selection, although necessary to keep in the analysis only diffuse parts of the sky, does not change the results and conclusions of the paper.

3. Analysing the data

3.1. Deriving the HI-correlated component spectrum

The HI-correlated dust emission is the dominant component at high galactic latitude at infrared/far-infrared/submillimeter wavelengths (except in the very low HI column density regions where the Cosmic Infrared Background becomes an important contribution, e.g. Lagache et al. 1999). One way to study the infrared to millimeter properties of the diffuse sky at high galactic latitude is therefore to concentrate on the emission correlated with the HI gas. We search here for the spatial/spectral variations of the infrared to millimeter emission with the HI gas column densities.

To compute the emission spectrum of the component associated with HI gas from low to large column densities, we use a differential method that removes, within statistical variance, any residual infrared emission that is not correlated

with the HI gas such as an isotropic component. We first select sky pixels according to their HI column density and sort them into sets of pixels bracketed by selected values of N_{HI} . Correlated HI emission spectra are then computed for each set of pixel k using the equation:

$$F_\nu(k) = \frac{\langle F \rangle_k - \langle F \rangle_0}{\langle N_{\text{HI}} \rangle_k - \langle N_{\text{HI}} \rangle_0} \quad (1)$$

where $\langle F \rangle_i$ corresponds to the mean emission computed for the set of pixels i , and $\langle N_{\text{HI}} \rangle_i$ to the mean HI column density for the same set of pixels. Note that all the data-sets used here are cosecant-law subtracted (see Sect. 2.5).

To keep high signal-to-noise ratio, only 5 sets of pixels are considered here, with increasing N_{HI} . The first set (labeled “0” in Eq. (1)), serves as the “reference” set and corresponds to the lowest column density regions (representing ~5% of the sky). We are thus left with 4 sets of pixels k with increasing N_{HI} and derive accordingly four mean spectra $F_\nu(k)$. The sets of pixels are selected on the cosecant-law removed HI emission that can be negative. For reference, the total mean HI column density (i.e. non cosecant-law subtracted) for the 4 bins are 3.3, 4.1, 5.6 and 9.9×10^{20} at/cm². By construction, the spectra are normalised to 10^{20} at/cm². Note that F in Eq. (1) represents alternatively the *DIRBE*, *FIRAS*, *DMR*, *WMAP*, free-free and synchrotron data.

3.2. Results

The four spectra are presented in Fig. 1 with the *DIRBE* data points at 100 and 140 μm , the *FIRAS* spectra (displayed only between 210 and 1000 μm), the *DMR* data points at 90, 53 and 31 GHz and the *WMAP* data points at 3.2, 4.9, 7.3 and 9.1 mm (all these data points are in black in Fig. 1). A zoom on the millimeter part of the figure is presented in Fig. 2. We fit the *DIRBE* 100, 140 μm and *FIRAS* spectra ($200 < \lambda < 500 \mu\text{m}$) with a modified Planck curve with a ν^2 emissivity law (the result of the fit is displayed in Fig. 1 and 2). We know that this fit is inconsistent with *FIRAS* data below ~500 GHz where an excess component is detected (Reach et al. 1995; Finkbeiner et al. 1999). However, discussing this component is not the goal of this paper. We only concentrate on the millimeter part on the spectra and how it relates to the far-infrared emission. It is important to note that this far-infrared dust emission has a stable spectrum, not changing with increasing opacity (Lagache et al. 1999). In this framework, the ν^2 modified black body is well representative and useful for comparison between spectral far-infrared and millimeter shapes³. This far-infrared dust emission extrapolated at millimeter wavelengths will be called the “stable thermal dust component”.

First, we see in Fig. 2 that there is a strong millimeter excess (with both *DMR* and *WMAP* data) with respect to the stable thermal dust component (i.e. the ν^2 modified black body). This excess decreases significantly (by a factor of about 5 at 3.2 mm) when the HI column density increases, although the far-infrared emission remains nearly constant (at the ~6%

¹ <http://lambda.gsfc.nasa.gov/product/map/>

² <http://www.eso.org/science/healpix>

³ The way we are fitting the far-infrared stable component is not critical since we focus on the variable millimeter emission.

Table 1. *WMAP*, free-free, synchrotron and stable thermal dust component emission (in $\text{W}/\text{m}^2/\text{sr}$, normalised to $10^{20} \text{ at}/\text{cm}^2$) in the four HI bins together with the residual emission (which is equal to *WMAP* – Free-free – Synchrotron – Stable thermal dust). The mean total HI column densities are $3.3, 4.1, 5.6$ and $9.9 \times 10^{20} \text{ at}/\text{cm}^2$ for the bin 1, 2, 3 and 4 respectively.

Component		3.2 mm	4.3 mm	7.9 mm	9.1 mm
<i>WMAP</i>	1	2.05×10^{-12}	6.15×10^{-13}	2.92×10^{-13}	2.19×10^{-13}
	2	1.52×10^{-12}	4.65×10^{-13}	2.25×10^{-13}	1.80×10^{-13}
	3	7.59×10^{-13}	2.26×10^{-13}	1.31×10^{-13}	1.27×10^{-13}
	4	7.22×10^{-13}	2.03×10^{-13}	1.34×10^{-13}	1.37×10^{-13}
Free-free	1	1.46×10^{-13}	1.02×10^{-13}	7.23×10^{-14}	6.03×10^{-14}
	2	1.14×10^{-13}	7.93×10^{-14}	5.65×10^{-14}	4.71×10^{-14}
	3	8.33×10^{-14}	5.79×10^{-14}	4.12×10^{-14}	3.44×10^{-14}
	4	7.36×10^{-14}	5.12×10^{-14}	3.64×10^{-14}	3.04×10^{-14}
Synchrotron	1	5.32×10^{-15}	4.28×10^{-14}	6.56×10^{-14}	7.60×10^{-14}
	2	3.57×10^{-14}	3.95×10^{-14}	5.67×10^{-14}	7.24×10^{-14}
	3	4.27×10^{-14}	3.40×10^{-14}	5.01×10^{-14}	6.76×10^{-14}
	4	3.79×10^{-14}	4.64×10^{-14}	6.19×10^{-14}	8.20×10^{-14}
Stable thermal dust	1	3.17×10^{-13}	3.95×10^{-14}	5.53×10^{-15}	1.86×10^{-15}
	2	2.81×10^{-13}	3.50×10^{-14}	4.90×10^{-15}	1.64×10^{-15}
	3	2.91×10^{-13}	3.62×10^{-14}	5.08×10^{-15}	1.71×10^{-15}
	4	3.66×10^{-13}	4.55×10^{-14}	6.39×10^{-15}	2.15×10^{-15}
Residue	1	1.58×10^{-12}	4.31×10^{-13}	1.48×10^{-13}	8.11×10^{-14}
	2	1.09×10^{-12}	3.12×10^{-13}	1.02×10^{-13}	5.89×10^{-14}
	3	3.41×10^{-13}	9.75×10^{-14}	3.42×10^{-14}	2.29×10^{-14}
	4	2.45×10^{-13}	5.94×10^{-14}	2.95×10^{-14}	2.20×10^{-14}

level). The far-infrared emission is dominated by the so-called Large Grain dust component. The millimeter excess, which changes rapidly with opacity, is thus not likely associated with this dust component.

We can go further by removing to the *WMAP* emission the corresponding free-free, synchrotron and stable thermal dust component contribution. The residual *WMAP* emission is shown in Figs. 1 and 2 (red stars) and detailed in Table 1. First, at each frequency, the residual emission exhibits a strong decrease (by about a factor of 5) with HI column densities (from bin 1 to 4). Second, the residual emission decreases from 3.2 to 9.1 mm in each HI bin. In Fig. 3 are shown the *WMAP* residual emissions for the 4 bins at 3.2, 4.9, 7.3 and 9.1 mm, normalised to the 90 GHz *DMR* residual emission (the 31 and 53 GHz *DMR* residual emissions have also been computed but are not displayed to avoid confusion. Results, although more noisy, are in very good agreement with *WMAP*). This figure shows that we do not detect any significant variations in the spectral shape of the residual emission⁴. Thus, the HI-normalised residual emission, although decreasing in amplitude with the HI column density, has a constant spectrum.

4. Discussion

To account for the galactic energy emitted from the mid-infrared to the submillimeter, it is necessary to have a broad dust size distribution from large grains down to large

molecules. For example, Désert et al. (1990) (see also Draine & Anderson 1985; Puget et al. 1995; Weiland et al. 1986; Siebenmorgen & Krügel 1992; Dwek et al. 1997 and more recently Li & Draine 2001) have proposed a consistent interpretation of both the infrared emission in diffuse HI clouds and the interstellar extinction curve using a model with three components: PAHs (Polycyclic Aromatic Hydrocarbons), Very Small Grains (VSGs) and Large Grains. PAHs and VSGs are small enough ($a \leq 10 \text{ nm}$) to experience significant temperature fluctuations after photon absorption. They emit over a wide range of temperatures and dominate the emission for $\lambda \leq 60 \mu\text{m}$. The Large Grain component is the more traditional dust component historically inferred from optical studies. These grains are in equilibrium with the incident radiation field with a temperature of about 17 K in the diffuse atomic medium (Boulanger et al. 1996). The Large Grain dust component is expected, at long wavelengths, to be proportional to the total amount of solid material. The large spatial variations of the infrared spectrum over the wavelengths range 12–60 μm have been interpreted as changes in the abundance of small grains (Boulanger et al. 1990; Laureijs et al. 1991; Bernard et al. 1993; Abergel et al. 1994). In particular, strong deficits of the transiently heated grains emitted at 60 μm are observed in dense interstellar clouds, these deficits being explained by grain-grain coagulation processes (e.g. Stepnik et al. 2003).

It has been shown in Sect. 3.2 that the HI-normalised residual *WMAP* emission (i.e. the excess above free-free and synchrotron contributions and the stable thermal dust component) is well traced at large scale by the HI gas and (1) exhibits a

⁴ This however will have to be quantified when smoothed *WMAP* data with error bars will be available.

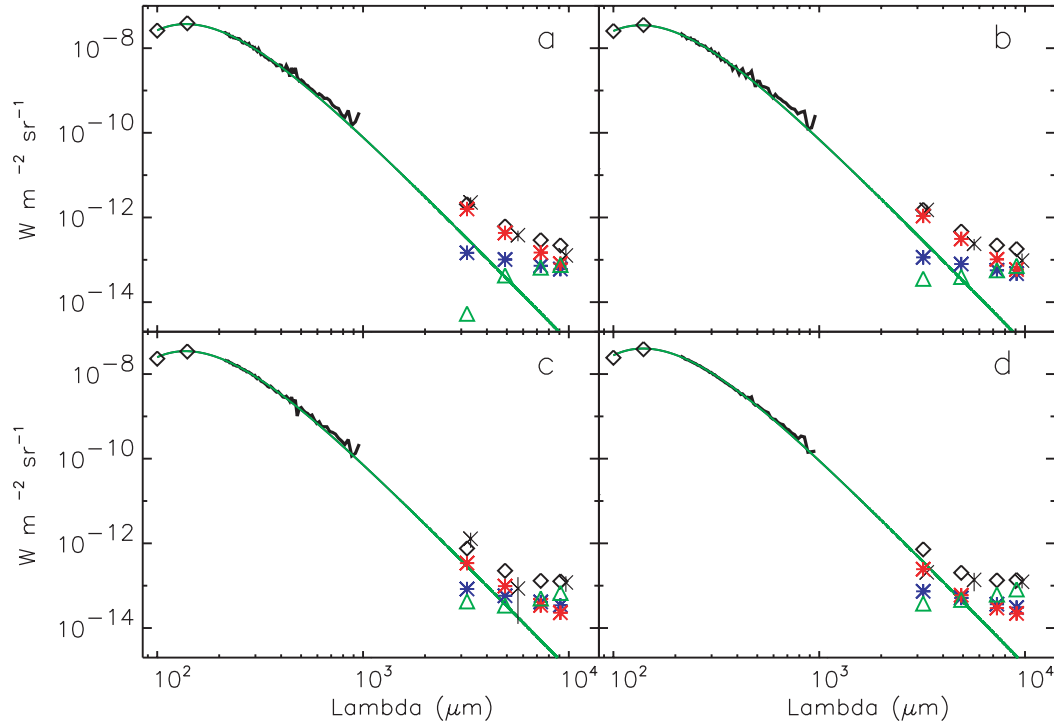


Fig. 1. Spectrum of the HI-correlated component normalised to 10^{20} at/cm 2 (with increasing $N(\text{HI})$ from **a**) to **d**). The black diamonds at 100 and 140 μm are the *DIRBE* data, the black curve is the *FIRAS* spectrum, the black crosses with error bars are the *DMR* data and the black triangles at 3.2, 4.9, 7.3 and 9.1 mm are the *WMAP* data. Also displayed are the free-free and synchrotron contributions (blue stars and green triangles respectively). The green continuous line is the result of a fit of the *DIRBE* 100, 140 μm and *FIRAS* spectra ($200 < \lambda < 500 \mu\text{m}$) with a modified Planck curve with a ν^2 emissivity law (the so-called stable thermal dust component). The residual *WMAP* emission (which is the *WMAP*-free-free – synchrotron – stable thermal dust component) is shown as red stars.

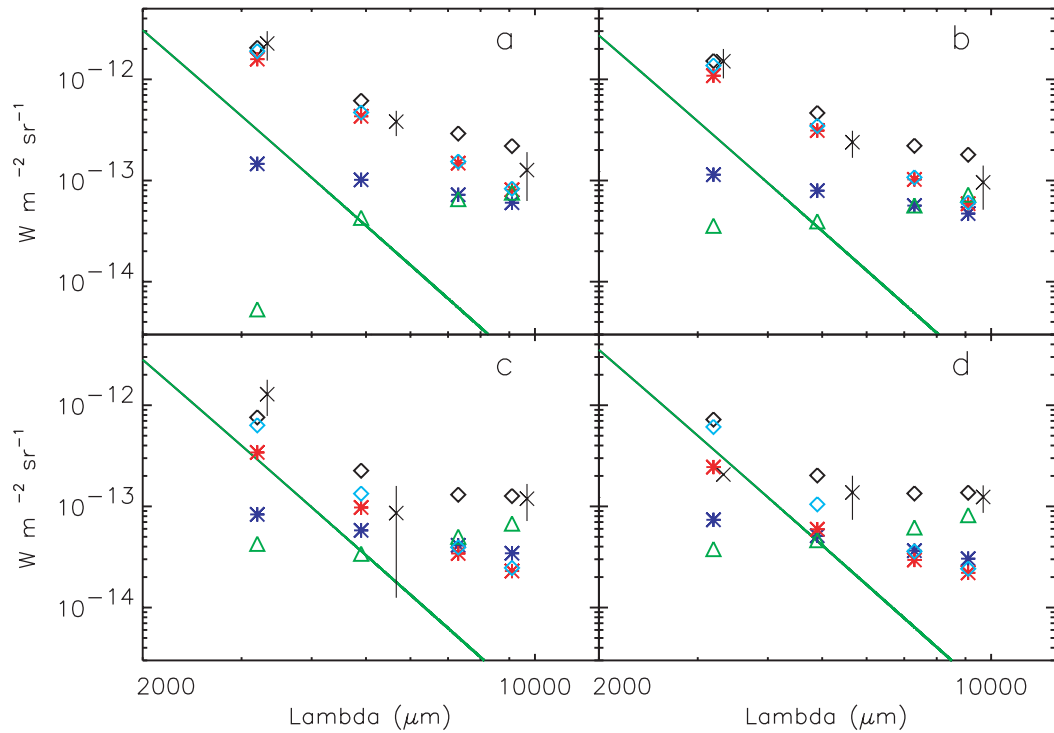


Fig. 2. Zoom on the millimeter part of Fig. 1. Symbols and colors are the same as in Fig. 1. Added is the residual *WMAP* emission after having removed only the free-free and synchrotron contributions (light-blue diamonds).

Table 2. Excess residual emission (νR_ν) at 3.2, 4.9, 7.3 and 9.1 mm with 240, 140, 100 associated brightnesses (in $\text{W}/\text{m}^2/\text{sr}$, normalised to 10^{20} at/cm^2) for the 4 HI bins. The $60 \mu\text{m}$ brightness is given for $|\beta| > 3^\circ$ and $|\beta| > 15^\circ$ to show that the decrease may not be due to any residual zodiacal light emission. Also given are the $60 \mu\text{m}$ brightnesses corresponding to the Very Small Grains dust component only (we have removed from the $60 \mu\text{m}$ emission, $I(60 \mu\text{m})$, the best ν^2 modified black body fit done on the Large Grain dust component).

	HI bin 1	HI bin 2	HI bin 3	HI bin 4
$\nu R_\nu(3.2 \text{ mm})$	1.58×10^{-12}	1.09×10^{-12}	3.41×10^{-13}	2.45×10^{-13}
$\nu R_\nu(4.9 \text{ mm})$	4.31×10^{-13}	3.12×10^{-13}	9.75×10^{-14}	5.94×10^{-14}
$\nu R_\nu(7.3 \text{ mm})$	1.48×10^{-13}	1.02×10^{-13}	3.42×10^{-14}	2.95×10^{-14}
$\nu R_\nu(9.1 \text{ mm})$	8.11×10^{-14}	5.89×10^{-14}	2.29×10^{-14}	2.20×10^{-14}
$\nu I_\nu(240 \mu\text{m})$	1.81×10^{-8}	1.63×10^{-8}	1.59×10^{-8}	1.83×10^{-8}
$\nu I_\nu(140 \mu\text{m})$	3.90×10^{-8}	3.54×10^{-8}	3.41×10^{-8}	3.90×10^{-8}
$\nu I_\nu(100 \mu\text{m})$	2.61×10^{-8}	2.54×10^{-8}	2.31×10^{-8}	2.43×10^{-8}
$\nu I_\nu(60 \mu\text{m}) \beta > 3^\circ$	1.16×10^{-8}	9.37×10^{-9}	7.18×10^{-9}	6.48×10^{-9}
$\nu I_{\nu\text{VSG}}(60 \mu\text{m}) \beta > 3^\circ$	9.24×10^{-9}	6.98×10^{-9}	4.94×10^{-9}	4.21×10^{-9}
$\nu I_\nu(60 \mu\text{m}) \beta > 15^\circ$	9.34×10^{-9}	7.23×10^{-9}	4.57×10^{-9}	4.92×10^{-9}
$\nu I_{\nu\text{VSG}}(60 \mu\text{m}) \beta > 15^\circ$	7.01×10^{-9}	4.83×10^{-9}	2.32×10^{-9}	2.65×10^{-9}

constant spectrum from 3.2 to 9.1 mm but (2) significantly decreases in amplitude when N_{HI} increases, contrary to the far-infrared emission (associated with the so-called stable thermal dust component) which stays rather constant (cf. Table 2). It is thus very likely that the residual *WMAP* emission is not associated with the Large Grain dust component. The decrease in amplitude resembles in fact to the decrease of the PAH/VSGs emission observed in dense interstellar clouds. By extrapolating the PAH/VSGs behaviour from dense interstellar clouds to the diffuse medium, we may expect, when increasing the HI column density, to decrease the PAH and VSGs proportion and thus the HI-normalised mid-infrared emission. If this is true, then the PAH/VSGs HI-correlated emission should decrease with HI column densities. This decrease, if present, is very hard to observe in the mid-infrared due to the strong residual interplanetary dust emission at large scale. On the *DIRBE* bands, only the $60 \mu\text{m}$ may be used. We have computed for the 4 HI bins the $60 \mu\text{m}$ HI-correlated emission with two different cuts in ecliptic latitude ($|\beta| > 3^\circ$ and $|\beta| > 15^\circ$). Although the absolute level of the $60 \mu\text{m}$ HI-correlated emission varies for the 2 cuts, we observe nearly the same significant decrease of the HI-normalised $60 \mu\text{m}$ emission with the HI column density (cf. Table 2). The $60 \mu\text{m}$ band may be contaminated by the Large Grain emission (30 to 40%, e.g. Désert et al. 1990). Therefore, we remove to the $60 \mu\text{m}$ emission the Large Grain contamination using the best ν^2 modified black body fit (Fig. 1). The observed decrease at $60 \mu\text{m}$ becomes even larger (Table 2). Although this result should be interpreted with care due to the zodiacal contamination at $60 \mu\text{m}$, it suggests that the *WMAP* residual emission is associated with the small transiently heated particles.

The previous results suggest the anomalous microwave component is associated with the transiently heated dust particles, but its exact physical mechanism remains to be found. On the possible models of the anomalous emission linked to the transiently heated particles are:

- The ‘‘spinning-dust’’ which is the rotational emission from very small dust grains (Draine & Lazarian, 1998a, 1998b). However, although the spinning dust emission is in good

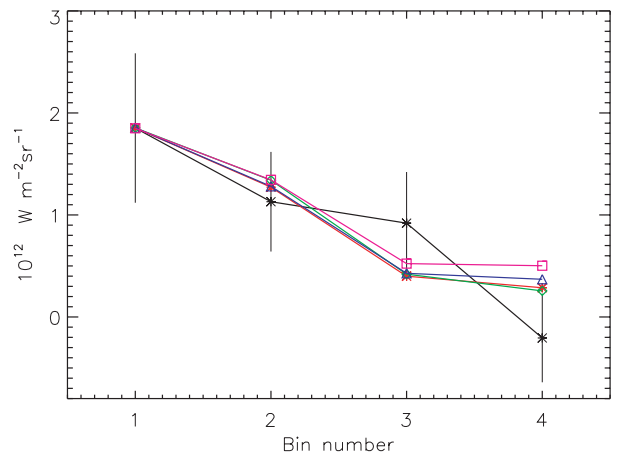


Fig. 3. HI-normalised residual *WMAP* emission at 3.2 (red), 4.9 (green), 7.3 (blue) and 9.1 (magenta) mm. All spectra are normalised on the *DMR* 90 GHz residual emission for the first HI bin (black points with error bars). The HI column density increases from bin 1 to 4 (from 3.3 to 9.9×10^{20} at/cm^2). No significant variations in the spectral shape of the residual emission is detected.

agreement with the *WMAP* emission at 7.3 and 9.1 mm, it is inconsistent with the 3.2 mm emission.

- The VSGs long-wavelength emission. VSGs are transiently heated when an ultraviolet photon is absorbed. The mean interval between successive ultraviolet photons is longer than the cooling time and thus, between 2 impacts, the temperature of the particles is very low (but is at least the CMB temperature). Such particles could therefore emit significant emission in the millimeter channels.

The models have large uncertainties linked to the unknown properties of the small particles. It is therefore very difficult to predict the exact contribution of the two in the millimeter.

Acknowledgements. The author thanks the *WMAP* team for having provided to the community beautiful data. Many thanks to J.-L. Puget and F. Boulanger for having carefully read this paper and for fruitful discussions. Thanks also to J.-P. Bernard for his help in the data manipulation.

References

- Abergel, A., Boulanger, F., Mizuno, A., & Fukui, Y. 1994, *ApJ*, 423, L59
- Banday A. J., & Wolfendale, A. W. 1991, *MNRAS*, 248, 705
- Banday, A. J., Dickinson, C., Davies, R. D., et al. 2003, *MNRAS*, submitted
- Bernard, J. P., Boulanger, F., & Puget, J.-L., 1993, *ApJ*, 277, 609
- Bennett, C. L., Smoot, G. F., & Hinshaw, G. 1992, 396, L7
- Bennett, C. L., Hill, R. S., Hinshaw, G., et al. 2003, *ApJ*, submitted
- Boulanger, F., Abergel, A., Bernard, J.-P., et al. 1996, *A&A*, 312, 256
- Boulanger, F., Falgarone, E., Puget, J.-L., & Helou, G. 1990, *ApJ*, 364, 136
- Désert, F.-X., Boulanger, F., & Puget, J.-L. 1990, *A&A*, 327, 215
- De Oliveira-Costa, A., Tegmark, M., Gutierrez, C., et al. 1999, *ApJ*, 527, L9
- De Oliveira-Costa, A., Tegmark, M., Finkbeiner, D., et al. 2002, *ApJ*, 567, 363
- Dickinson, C., Davies, R. D., & Davis, R. J. 2003, *MNRAS*, 341, 369
- Draine, B. T., & Anderson, N. 1985, *ApJ*, 292, 494
- Draine, B. T., & Lazarian, A. 1998a, *ApJ*, 494, L19
- Draine, B. T., & Lazarian, A. 1998b, *ApJ*, 508, 157
- Draine, B. T., & Lazarian, A. 1999, *ApJ*, 512, 740
- Dwek, E., Arendt, R. G., Fixsen, D. J., et al. 1997, *ApJ*, 475, 565
- Finkbeiner, D., Davis, M., & Schlegel, D. J. 1999, *ApJ*, 524, 867
- Finkbeiner, D., Schlegel, D. J., Frank, C., & Heiles, C. 2002, *ApJ*, 566, 898
- Finkbeiner, D. 2003, *ApJS*, 146, 407
- Gaustad, J. E., Mc Cullough, P. R., Rosing, W. R., & Buren, D. V. 2001, *PASP*, 113, 1326
- Haffner, L. M. 1999, Ph.D. Thesis, University of Wisconsin
- Hartmann, D. 1994, Ph.D. Thesis, University of Leiden
- Hartmann, D., & Burton, W. B. 1997, *Atlas of galactic neutral hydrogen* (Cambridge, New-York: Cambridge University Press), ISBN 0521471117
- Haslam, C. G. T., Salter, C. J., Stoffel, H., & Wilson, W. 1982, *A&AS*, 47, 1
- Kogut, A., Banday, A. J., Bennett, C. L., et al. 1996, *ApJ*, 460, 1
- Kogut, A. 1999, in *Microwave Foregrounds*, ed. A. De Oliveira Costa, & M. Tegmark, *ASP Conf. Ser.*, 181, 91
- Lagache, G., Abergel, A., Boulanger, F., & Puget, J.-L. 1998, *A&A*, 333, 709
- Lagache, G., Abergel, A., Boulanger, F., et al., 1999, *A&A*, 344, 322
- Lagache, G. 2003, *Absolute photometric calibration of Planck/HFI high-frequency channels on the Galaxy: Application to Archeops data*, *A&A*, submitted
- Laurejis, R. J., Clark, F. O., & Prusti, T. 1991, *ApJ*, 372, 185
- Li, A., & Draine, B. T. 2001, *ApJ*, 554, 778
- Puget, J. L., Léger, A., & Boulanger, F. 1985, *A&A*, 142, L19
- Reach, W. T., Dwek, E., Fixsen, D. J., et al. 1995, *ApJ*, 451, 188
- Reynolds, R. J., Tufte, S. L., Haffner, L. M., et al. 1998, *PASA*, 15, 14
- Siebenmorgen, R., & Krügel, E. 1992, *A&A*, 259, 614
- Stepnik, B., Abergel, A., Bernard, J.-P., et al. 2003, *A&A*, 398, 551
- Weiland, J. L., Blitz, L., Dwek, E., et al. 1986, *ApJ*, 306, L101